

Jülich GmbH (FZJ) and Karlsruher Institut für Technologie (KIT) (Riese et al., 2014; Friedl-Vallon et al., 2014).

GLORIA is the direct successor of two successful lines of infrared limb sounders. One of these is the Cryogenic Infrared Spectrometers and Telescopes for the Atmosphere (CRISTA), which was developed originally as a satellite instrument and saw two orbital deployments during Space Shuttle missions in 1994 and 1997 (Offermann et al., 1999; Riese et al., 1997, 2002; Grossmann et al., 2002). Due to the success of these missions, an airborne adaptation, called CRISTA-NF (for “New Frontiers”), was developed later and deployed on the M-55 Geophysica research aircraft (Kullmann et al., 2004).

The other line of GLORIA’s heritage is the Michelson Interferometer for Passive Atmospheric Sounding (MIPAS). Apart from the 10-year deployment of MIPAS on board the European Space Agency’s Environmental Satellite (Envisat) (Fischer et al., 2008), MIPAS has also been highly successful as a balloon instrument (Friedl-Vallon et al., 2004). The airborne MIPAS-STR (for “Stratospheric Aircraft”) adaptation (Piesch et al., 1996), also developed for the M-55 Geophysica, can be seen as GLORIA’s direct precursor, alongside CRISTA-NF.

CRISTA-NF and MIPAS-STR were both conceived for observations in the UTLS, but with different priorities. The former was primarily designed for the study of transport and mixing processes. CRISTA-NF data from the African Monsoon Multidisciplinary Analyses (AMMA) and Reconciliation of Essential Process Parameters for an Enhanced Predictability of Arctic Stratospheric Ozone Loss and its Climate Interactions (RECONCILE) measurement campaigns have been used to derive trace gas mixing ratios with unprecedented vertical resolution and along-track sampling (Ungermann et al., 2012, 2013; Kalicinsky et al., 2013; Weigel et al., 2012). MIPAS-STR, on the other hand, was designed for a chemistry-centred analysis, offering a higher spectral resolution in order to derive more elusive trace gases (Woiwode et al., 2012), at the cost of lower spatial sampling.

Calibration noise suppression for GLORIA

T. Guggenmoser et al.

Title Page

Abstract

Introduction

Conclusions

References

Tables

Figures



Back

Close

Full Screen / Esc

Printer-friendly Version

Interactive Discussion



Calibration noise suppression for GLORIA

T. Guggenmoser et al.

Title Page

Abstract

Introduction

Conclusions

References

Tables

Figures



Back

Close

Full Screen / Esc

Printer-friendly Version

Interactive Discussion



Compared with CRISTA-NF and MIPAS-STR, GLORIA incorporates a number of advancements that greatly enhance and diversify its UTLS sounding capabilities. As an imager, it is capable of recording complete vertical profiles in a single measurement, without the need for elevation scanning. This greatly improves the spatial sampling of measurements. Another main feature of GLORIA is its ability to operate in either of two measurement modes: a chemistry mode (CM) with high spectral sampling (0.0625 cm^{-1}) and dynamics mode (DM) with lower spectral sampling (0.625 cm^{-1}) but higher spatial sampling.

The CM can be used for the retrieval of trace gases with faint or not easily separable spectral signatures, such as ethane (C_2H_6), using the Karlsruhe Optimized and Precise Radiative Transfer Algorithm (KOPRA) (Stiller, 2000; Höpfner et al., 1998). The DM measurements are ten times as quick. Together with GLORIA's ability to pan the line of sight between measurements, it is possible to collect DM datasets suited for 3-D tomographic trace gas retrieval algorithms. This has been demonstrated via simulation (Ungermann et al., 2010, 2011) and applied to measurement data (Kaufmann et al., 2014). Measurements recorded in DM are all processed using the Juelich Rapid Spectral Simulation Code (Hoffmann et al., 2008) version 2 (JURASSIC2), together with the Juelich Tomographic Inversion Library (JUTIL) (Ungermann et al., 2014).

In this paper, several advancements in the processing of GLORIA spectra are presented, particularly the derivation of the instrument calibration function. Previously, the calibration parameters were found by treating each pixel of the focal plane array individually. New techniques have now been developed to generate the calibration parameters which make use of the spatial homogeneity of the individual images. With this new approach, the noise present in the gain and offset parameters and resulting artefacts in the calibrated radiances are significantly reduced.

These new algorithms were developed in tandem with a new data processing system which incorporates previously separate processing stages, resulting in a semi-automated processing chain. Once the calibration parameters are found, it is now pos-

Calibration noise suppression for GLORIA

T. Guggenmoser et al.

Title Page

Abstract

Introduction

Conclusions

References

Tables

Figures



Back

Close

Full Screen / Esc

Printer-friendly Version

Interactive Discussion



express the radiance as a function of the OPD. This is referred to as the L0 processing step (Kleinert et al., 2014). The resulting spatial interferograms are, up to the instrument function, the Fourier transform of the spectrum of recorded radiances (Beer, 1992).

The L1 processing step derives absolute spectral radiances from the L0 data. The first and most straightforward step is to apply the Fourier transform. Because GLORIA records two-sided interferograms, the resulting spectra are complex-valued. If the two interferogram sides were perfectly symmetric, the imaginary part would vanish. This is not the case for three principal reasons: firstly, noise will not be symmetric around the point of zero OPD. Secondly, the point of zero OPD is never exactly sampled by the instrument in practice, although this effect can be compensated for by an interferogram alignment correction at the L0 stage. Thirdly and most importantly, because GLORIA does not operate near absolute zero temperature, the interferograms contain emission and absorption signatures from various parts of the instrument, which enter the signal at different phase angles relative to each other (Kleinert and Trieschmann, 2007).

The radiometric calibration, i.e. the inversion of the instrument function, is performed assuming \mathbb{C} -linear behaviour. If $\tilde{y}(\nu)$ is the spectral radiance at the spectral sample ν , the spectrum obtained from the measurements is

$$y(\nu) = a(\nu)\tilde{y}(\nu) + b(\nu), \quad (1)$$

with a and b being the complex radiometric gain and offset parameters. The advantage of this complex calibration scheme is that the non-atmospheric signal components are automatically removed, without having to determine their individual magnitudes and phase angles (Revercomb et al., 1988).

As known reference radiation sources, the GLORIA instrument carries two blackbodies with it, BBH and BBC (for “hot” and “cold”, respectively). They emit spatially homogeneous infrared radiation at their respective stabilised temperatures (Monte et al., 2013; Olschewski et al., 2013). Using measurements from these blackbody sources, as well as upward-pointing deep space (DS) measurements, the parameters a and b for each pixel and spectral sample can be obtained by either of two methods. The

cumvents the problem of residual trace gas emissions in the DS measurements, and because it can serve as a consistency test for the parameters derived from BB-DS.

We found that the spatial variation of the real part of the NCO over the detector can be reproduced by a simple pseudo-hyperbola of the form

$$f_{x_c, y_c, a, b, c, d}(x, y) = c + \left(b^4 + \left(a^2 \left((x - x_c)^2 + (y - y_c)^2 \right) \right)^2 \right)^{1/4} \quad (7)$$

The parameters $x_c, y_c, a, b, c, d \in \mathbb{R}$ describe the position and shape of the pseudo-hyperbola, while x and y are the coordinates of the detector pixels. A series of higher-dimensional functions was also tested but did not yield better results than Eq. (7).

While imperfect in certain spectral ranges, this function lets us correct the more serious artefacts in the following manner. First, the radiometric gain and offset are determined according to Eqs. (4) and (5), and from these two the NCO function. Then, individually for each spectral sample, a least squares fit is performed to find the pseudo-hyperbola that best reproduces its real part. This real part is then replaced by the smooth pseudo-hyperbola. Using the new NCO function and the original calibration measurements, the radiometric gain function is updated for consistency.

A representative calibration sequence from the TACTS measurement campaign has been chosen to illustrate the effects of this method. From the BB and DS measurements, the calibration parameters IG and NCO have been determined, both via BB-BB and via BB-DS calibration. Both sets of parameters have then been subjected to the pseudo-hyperbola fit correction as described above, yielding a total of four sets of calibration parameters to compare.

The comparison of the NCO real parts for the spectral sample at 791.875 cm^{-1} is shown in Fig. 2. The non-fitted BB-DS calibration serves as a reference. The symmetric, ring-like shape of the NCO function which motivated the pseudo-hyperbola is recognisable in the uncorrected BB-DS and BB-BB data. However, the BB-BB image is much more noisy than the BB-DS reference, and differs from it both by a homogeneous bias and by a large number of small-scale structures. These structures, which caused

Calibration noise suppression for GLORIA

T. Guggenmoser et al.

Title Page

Abstract

Introduction

Conclusions

References

Tables

Figures



Back

Close

Full Screen / Esc

Printer-friendly Version

Interactive Discussion



**Calibration noise
suppression for
GLORIA**

T. Guggenmoser et al.

Title Page

Abstract

Introduction

Conclusions

References

Tables

Figures



Back

Close

Full Screen / Esc

Printer-friendly Version

Interactive Discussion



artefacts in the L2 processing stage, are removed by the pseudo-hyperbola fit. The bias and smoothly varying difference still remains, but this kind of calibration error can be more easily handled by the trace gas retrieval algorithms. Because the IG and NCO functions are interdependent, updating the BB-BB IG with the corrected NCO removes similar structures from it, as shown in Fig. 3.

The pseudo-hyperbola function cannot reproduce the NCO for all spectral samples, as shown in Fig. 4 for the one at 840 cm^{-1} . Here, the difference between the BB-DS NCO with and without the correction shows ring-like structures. However, the improvements to the BB-BB calibration over the rest of the spectrum outweigh the cost of these artefacts, which only persist for a limited number of samples.

Following the L1 processing step, the spectra are currently averaged over one row to reduce stochastically independent noise for the L2 processing. For this application, the average over each row of the NCO is an interesting diagnostic for the pseudo-hyperbola method. Figure 5 shows this quantity. Comparing the magnitude of the removed structures (in the order of $10^{-7}\text{ W cm}^2\text{ cm sr}^{-1}$ in the centre of the detector) with the magnitude of recorded atmospheric spectra, the artefacts would introduce a spatially uncorrelated error of up to nearly 8 % at this wavenumber for the BB-BB calibration unless corrected by the pseudo-hyperbola.

4 Calibration noise mitigation based on principal component analysis

4.1 Background and motivation

As shown in the previous section, GLORIA's DS calibration measurements are spatially highly correlated – each pixel on the detector records a very similar scene. The same is true for BB measurements: owing to the homogeneity of the radiation source (Olschewski et al., 2013), the main spatial variation in these measurements stems from the radiative instrument background.

Calibration noise suppression for GLORIA

T. Guggenmoser et al.

Title Page

Abstract

Introduction

Conclusions

References

Tables

Figures

◀

▶

◀

▶

Back

Close

Full Screen / Esc

Printer-friendly Version

Interactive Discussion



Let us assume that all pixels had the same response function. We could then pretend that the individual spectra within a calibration image were a series of measurements from the same detector, each time exposed to a slightly varying scene.

To put this in more mathematical terms, we have reason to suspect that the observed calibration scenes do not actually contain as many meaningful degrees of freedom as there are samples recorded by the instrument. If each of the n pixels' spectrum consists of p partially correlated complex samples, this means we could find a way to instead represent it using a smaller, but uncorrelated set of $p' < p$ complex numbers. Such a transformation can be achieved by principal component analysis (PCA, e.g. Jolliffe, 2002). The PCA is a linear basis transformation yielding the original data in terms of a new orthonormal basis, composed of the p eigenvectors of its covariance matrix and sorted in order of decreasing contribution to the total variance. These vectors are the “principal components”. Contributions to the original data which are fully uncorrelated, such as white noise, are distributed evenly among these principal components, so that reconstructing the data from a truncated set of p' components will ideally reduce the sample noise SD $\sigma(v)$ by a factor of

$$\frac{\sigma_p(v)}{\sigma_{p'}(v)} = \sqrt{\frac{p}{p'}} \quad (8)$$

However, in practice, the relation holds true only asymptotically for large n because the ability to separate noise from signal depends on the number of measurements available for the decomposition (e.g. Pyatykh et al., 2013). A more realistic estimate, on the basis of a simulated white noise data set, will be shown in Sect. 4.3.

PCA-based methods for the removal of noise from Fourier transform spectrometer measurements have been investigated in great detail (Antonelli et al., 2004), and have been applied with great success for the operational data compression and noise suppression for L1 products, e.g. for the Infrared Atmospheric Sounding Interferometer (IASI, August et al., 2012). GLORIA's imaging capabilities, in combination with the homogeneity of calibration scenes, enable the use of single- or averaged-image

Calibration noise suppression for GLORIA

T. Guggenmoser et al.

Title Page

Abstract

Introduction

Conclusions

References

Tables

Figures



Back

Close

Full Screen / Esc

Printer-friendly Version

Interactive Discussion



decomposition, as opposed to decomposition based on a training set of previous measurements. Note that PCA is usually formulated in a way that applies to real-valued data sets. In the following, we will use a straightforward generalisation to complex vector spaces. This has the implication that the covariance matrix of the data set is complex-valued, which makes it less readily interpreted. However, because the covariance matrix is self-adjoint, its main diagonal and its eigenvalues remain real numbers, so the components can still be ordered in the regular fashion.

4.2 Data preconditioning and application of PCA

We start with a matrix $\mathbf{X} \in \mathbb{C}^{n \times p}$ containing either a BB or DS data set in Fourier transformed, but not radiometrically calibrated form. The calibration data sets are obtained from averaging over all available single measurements of the same calibration source during one calibration sequence. The DS measurements have additionally been subjected to the trace gas emission removal technique (Kleinert et al., 2014). Again, n is the number of pixels, while p is the number of spectral samples considered. In this section, we have chosen the spectral range between 780 and 1450 cm^{-1} . The calibration measurements are processed at the dynamics mode sampling of 0.625 cm^{-1} , therefore $p = 1072$. For technical reasons, the topmost line of pixels is not considered, therefore $n = 6096$.

The relation with the true radiance image $\hat{\mathbf{X}}$ as seen by the detector can be expressed as

$$\mathbf{X} = \mathbf{G} \odot \hat{\mathbf{X}}, \quad (9)$$

where $\mathbf{G} \in \mathbb{C}^{n \times p}$ is the instrument gain matrix, and the symbol \odot was chosen to represent the Hadamard (entrywise) matrix product. In the case where \mathbf{X} is a DS data set, $\hat{\mathbf{X}}$ is dominated by the NCO, potentially with minor contributions from insufficiently removed residual trace gas signatures. If \mathbf{X} is a BB data set, the true image $\hat{\mathbf{X}}$ contains the NCO and the nearly homogeneous blackbody radiation.

Calibration noise suppression for GLORIA

T. Guggenmoser et al.

Title Page

Abstract

Introduction

Conclusions

References

Tables

Figures

◀

▶

◀

▶

Back

Close

Full Screen / Esc

Printer-friendly Version

Interactive Discussion



Principal component analysis can only be sensibly performed on a series of measurements of the same zero-average random variables of similar variance. In order to be able to apply PCA for noise suppression, the data set \mathbf{X} needs to be brought into a form which closely resembles this. To this end, the pixel response has to be normalised, i.e. the Hadamard inverse of the matrix \mathbf{G} needs to be applied to the measurements. This poses a fundamental problem, as the purpose of the calibration measurements is to obtain this matrix, and it is therefore naturally not known at this point.

We solve this problem by the following process. First, a PCA of the blackbody and deep space measurements is performed without gain normalisation, with a subsequent reconstruction using 20 covariance eigenvectors. These spectra, \mathbf{X}'_{BB} and \mathbf{X}'_{DS} are now used to infer an approximation of the gain matrix:

$$\mathbf{G}' = \Phi \left(\tilde{\mathbf{B}} \odot \left(\mathbf{X}'_{\text{BB}} - \mathbf{X}'_{\text{DS}} \right) \right), \quad (10)$$

where $\tilde{\mathbf{B}}$ contains the theoretically calculated inverse Planck radiances corresponding to the blackbody temperature. To avoid confusion with the ordinary matrix inverse, a tilde denotes inversion with respect to the Hadamard product. For the purposes of normalisation, multiplication with the inverse Planck radiances is not strictly necessary, but facilitates the physical interpretation of intermediate results. The function Φ is a Kaiser window which acts as a smoothing function on each row of the matrix. Its purpose is to keep noise and signal variance out of the normalisation matrix.

Using the entrywise inverse of the matrix \mathbf{G}' , the blackbody and deep space measurements can now be normalised:

$$\mathbf{X}'' = \tilde{\mathbf{G}}' \odot \mathbf{X}'. \quad (11)$$

To further reduce the variation that needs to be decomposed by the PCA, the NCO pseudo-hyperbola from Sect. 3 is fitted to the normalised deep space measurement at each spectral sample and then subtracted. Afterwards, the remaining mean value of each spectral sample is computed and subtracted as well, yielding the new matrix \mathbf{X}''' .

Calibration noise suppression for GLORIA

T. Guggenmoser et al.

Title Page

Abstract

Introduction

Conclusions

References

Tables

Figures

◀

▶

◀

▶

Back

Close

Full Screen / Esc

Printer-friendly Version

Interactive Discussion



This matrix now fulfills almost all the conditions necessary for the PCA. What is still missing is the normalisation of the individual spectral samples. Several methods exist to achieve this, the most simple of which being to divide each spectral sample by its sample SD. We opted for a method that approximates the spectral noise profile. A new reconstruction of the blackbody matrix is performed, based on the original decomposition, this time using 400 principal components. The difference between the original and the reconstructed spectrum is then used to normalise the noise variance of the matrix \mathbf{X}''' , under the assumption that the reconstruction error can be used as a proxy for the noise profile:

$$\mathbf{Y} = \mathbf{N}^{-1} \mathbf{X}''', \quad (12)$$

where $\mathbf{N} \in \mathbb{C}^{p \times p}$ contains the SD of the calculated difference on the main diagonal.

Finally, the PCA is performed on \mathbf{Y} by way of a complex singular value decomposition (SVD):

$$\mathbf{Y} = \mathbf{USV}^* = \mathbf{TV}^*. \quad (13)$$

Here, $\mathbf{U} \in \mathbb{C}^{n \times n}$ and $\mathbf{V} \in \mathbb{C}^{p \times p}$ contain the left- and right-singular vectors, respectively, and $\mathbf{S} \in \mathbb{C}^{n \times p}$ is a rectangular diagonal matrix which contains the singular values. The squares of the singular values are eigenvalues of the covariance matrix $\mathbf{Y}^* \mathbf{Y}$, the rows of \mathbf{V}^* contain the orthonormal eigenvectors and the rows of the product $\mathbf{T} = \mathbf{US}$ contain the linear factors, i.e. the coordinates of each row of \mathbf{Y} in the new basis defined by \mathbf{V} . A truncated reconstruction \mathbf{X}_P of \mathbf{X} using P covariance eigenvectors can now be obtained by first reconstructing \mathbf{Y} using truncated matrices \mathbf{S}_P and \mathbf{V}_P , then inverting the normalisation steps performed before.

After the procedure is finished, it is repeated once, starting with the original data set \mathbf{X} . The new decomposition (13) for the BB and DS measurements is now used instead of the initial PCA to estimate the gain matrix and pseudo-hyperbola more accurately. An iterative approach using successive repetitions of the procedure was considered, but did not yield improved results.

presumably because they are less spatially homogeneous. In any case, the contaminated spectral range cannot be used, so the quality of its reconstruction is not crucial.

4.4 Covariance eigenvalues

Another avenue for diagnostics is provided by inspection of the singular values s_i , i.e. the main diagonal elements of the matrix \mathbf{S} from Eq. (13), whose squares are the covariance matrix eigenvalues. The cumulative sum of the squared singular values, normalised by the total sum, is the relative total variance of each variable restored in the reconstruction:

$$\frac{\sigma_P^2}{\sigma^2} = \frac{\sum_{i=0}^P s_i^2}{\sum_{i=0}^p s_i^2} = \frac{\text{tr}(\mathbf{S}_P^T \mathbf{S}_P)}{\text{tr}(\mathbf{S}^T \mathbf{S})} \quad (14)$$

As was mentioned in Sect. 4.1, the distribution of white noise among the PCA vectors depends on the dimensionality of the data set. To estimate the performance of our method, we have generated a matrix $\mathbf{X}_{\text{syn}} \in \mathbb{C}^{6096 \times 1072}$. The real and imaginary parts of the matrix entries were drawn independently from a standard normal distribution.

Figure 10 shows the first 70 normalised covariance eigenvalues for the DS spectrum from Fig. 6, the BB data set from Fig. 7, and the white noise matrix \mathbf{X}_{syn} . The cumulative sum of the first 30 eigenvalues is shown in Fig. 11.

For the DS spectra, the first five principal components already account for more than half of the variation in the measurement. Using 20 vectors, this figure increases to 60 %. It should be noted here that this is the variance after the normalisation procedure, i.e. most of the variation over the detector has already been removed. The spectrum reconstructed here is a combination of the detector noise, a correction to the assumed pseudo-hyperbola shape in the real part and the imaginary part of the spectrum.

The BB data set can be reconstructed to 90 % of the total variance from as few as 14 principal components. Because the BB spectra contain the same background as

Calibration noise suppression for GLORIA

T. Guggenmoser et al.

Title Page	
Abstract	Introduction
Conclusions	References
Tables	Figures
◀	▶
◀	▶
Back	Close
Full Screen / Esc	
Printer-friendly Version	
Interactive Discussion	



the DS as well as the much brighter blackbody radiation, the total variance is higher. However, the blackbody radiation, which accounts for most of the signal, is easily reconstructed due to its homogeneity.

The synthetic noise is reconstructed much more linearly than the BB and DS measurements, but the covariance eigenvalues still decrease slightly for successive components. This is the expected non-uniform noise distribution which motivated the simulation. The contribution of successive principal components starts at 0.19% and decreases to 0.16% for the 70th component. The last eigenvalue (not shown in the plots) is 3.2×10^{-4} , an order of magnitude smaller than the first one. The mean eigenvalue is $1/1072 \approx 9.3 \times 10^{-4}$, the expected contribution of each single component if the noise variance was distributed evenly.

4.5 Comparison with low-pass filtering

Another useful method for noise mitigation of GLORIA calibration measurements is a simple low-pass filtering (LPF) of the spectra. Note that, in this context, LPF refers to low and high frequencies in the Fourier space associated with the spectrum, not with the recorded signal. This space can be identified with the interferogram space. Applying an LPF to the spectrum is therefore equivalent to a shortening of the interferogram in combination with a Fourier interpolation of the spectrum.

Both methods employ the same general principle in that they are compression methods: the spectra are decomposed and components are discarded according to their expected signal-to-noise ratio. However, the mechanism by which this is achieved is different. The BB and DS measurements contain the instrument background and calibration blackbody radiation, both of which are spectrally slowly varying signals without discernible emission or absorption lines. This motivates and justifies the use of the LPF, which discards the higher frequencies, i.e. the rapidly varying components, because they can be expected to contain little or no signal, but contribute equally to the noise level. The PCA method decomposes the data into uncorrelated components and

Calibration noise suppression for GLORIA

T. Guggenmoser et al.

Title Page

Abstract

Introduction

Conclusions

References

Tables

Figures



Back

Close

Full Screen / Esc

Printer-friendly Version

Interactive Discussion



retains only the most significant ones, discarding those that contribute little to the total variance of each spectral sample.

Because of the qualitatively different effects the two methods have on the data, a quantitative comparison of PCA and LPF proved difficult. In the following, we will make a qualitative comparison between a PCA reconstruction from 20 principal components (PCA-20) and a low-pass filter which dampens all but the 512 lowermost frequencies (LPF-512). As Fig. 11 shows, the first 20 PCA vectors reconstruct the simulated noise variance to 3.6 %, implying a reduction of the noise SD by over 80 %.

Figure 12 shows a reconstruction of a spectrum subjected to the PCA-20 and LPF-512 methods, as well as a third one, where the signal was first reconstructed from the principal components and subsequently low-pass-filtered. For a more detailed inspection of the differences, Figs. 14 and 13 show the same spectra within a reduced wavenumber range.

The LPF-512 method effectively reduces the interferogram length from 8000 to 1024 real samples, i.e. it retains 512 of 4001 complex modes. Assuming a uniform noise distribution among the modes, this implies a noise level reduction of 2.8 : 1, while for the PCA-20 method we expect a ratio of 5 : 1 from the simulation in Sect. 4.4. A more fundamental difference, regardless of the number of principal components, is that the noise removed by the PCA method does not have a high-frequency bias, which is why the smoothing effect is less pronounced.

This difference between the PCA and the low-pass methods is further illustrated by Fig. 15, which shows the magnitude of the complex reconstruction error in Fourier space, for the LPF-512, PCA-20 and combined methods. The reconstruction error for the pure low-pass method is an order of magnitude smaller for the lowermost frequencies, corresponding to the low-pass window employed. The PCA method, on the other hand, distributes the reconstruction error more uniformly across the spectrum. This is also true for the combined method as long as the number of principal components is small. For larger numbers, the PCA-reconstructed spectrum approaches the original spectrum, and the combined reconstruction accordingly the LPF-512 method.

Calibration noise suppression for GLORIA

T. Guggenmoser et al.

Title Page

Abstract

Introduction

Conclusions

References

Tables

Figures



Back

Close

Full Screen / Esc

Printer-friendly Version

Interactive Discussion



The benefit of the combined approach is that most of the noise variance is already subtracted before the low-pass is applied, and therefore the undesired interpolation of the low-frequency noise modes avoided. This results in a smooth calibration spectrum without the smoothing artefacts in the shape of slow oscillations.

5 Conclusions and outlook

One of the GLORIA limb sounder's key features is its imaging capability. In this paper, we presented two new ways to exploit this feature for the suppression of noise and certain artefacts in the calibration measurements.

The first technique was the empirical spatial characterisation of GLORIA's radiometric background, which helps identify and alleviate issues stemming from noisy calibration measurements and an imperfect nonlinearity correction. Fitting a pseudo-hyperbola to the gain-calibrated radiometric offset allows us to use both blackbodies to generate calibration data of decent quality. Without the fit, the amplification of these errors by extrapolation of the offset would cause artefacts in the calibrated radiances, which would severely impact the L2 processing.

We could significantly reduce the noise level of BB and DS calibration spectra by exploiting the spatial correlation of GLORIA's calibration scenes. Via truncated principal component analysis, we were able to reconstruct the original measurements while reducing the noise level significantly. Compared with low-pass smoothing, an alternative option for GLORIA spectra, the PCA reconstruction is less smooth, but subtracts high- and low-frequency noise variance equally. By contrast, low-pass filters retain the low-frequency noise components, resulting in slowly oscillating perturbations in the result. A combined approach, where a low-pass smoothing is performed on previously PCA-compressed spectra, yielded the best results with suppressed low-frequency noise.

We expect that the techniques presented in this paper can also be generalised and transferred to other instruments with a focal plane array and similar absolute radiance calibration. The utility of the PCA-based method for other instruments would likely de-

Calibration noise suppression for GLORIA

T. Guggenmoser et al.

Title Page

Abstract

Introduction

Conclusions

References

Tables

Figures



Back

Close

Full Screen / Esc

Printer-friendly Version

Interactive Discussion



pend on the number of pixels available for each measurement, as well as the homogeneity of the calibration scenes.

In parallel with the new noise suppression techniques, a new L0/L1 data processing chain was developed. This chain enables high-performance processing of raw data into L1 spectra once the calibration parameters have been provided. Determining the parameters is difficult to automate, and is therefore still done under human supervision. Work on the integration of this task into the processing chain is currently in progress.

Acknowledgements. The GLORIA instrument was mainly funded by the Helmholtz Association. We thank the whole GLORIA instrument team for their role in developing the hardware and software, as well as planning and executing the measurement campaigns. Acknowledgments also go to Myasishchev Design Bureau and the German Aerospace Centre (DLR-FX), who operate GLORIA's carrier aircraft.

The service charges for this open access publication have been covered by a Research Centre of the Helmholtz Association.

References

- Antonelli, P., Revercomb, H. E., Sromovsky, L. A., Smith, W. L., Knuteson, R. O., Tobin, D. C., Garcia, R. K., Howell, H. B., Huang, H.-L., and Best, F. A.: A principal component noise filter for high spectral resolution infrared measurements, *J. Geophys. Res.*, 109, D23102, doi:10.1029/2004JD004862, 2004. 12660
- August, T., Klaes, D., Schlüssel, P., Hultberg, T., Crapeau, M., Arriaga, A., O'Carroll, A., Copens, D., Munro, R., and Calbet, X.: IASI on Metop-A: operational Level 2 retrievals after five years in orbit, *J. Quant. Spectrosc. Ra.*, 113, 1340–1371, 2012. 12660
- Beer, R.: *Remote Sensing by Fourier Transform Spectrometry*, vol. 170, Wiley-Interscience, 1992. 12654
- Fischer, H., Birk, M., Blom, C., Carli, B., Carlotti, M., von Clarmann, T., Delbouille, L., Dudhia, A., Ehhalt, D., Endemann, M., Flaud, J. M., Gessner, R., Kleinert, A., Koopman, R., Langen, J., López-Puertas, M., Mosner, P., Nett, H., Oelhaf, H., Perron, G., Remedios, J.,

12669

AMTD

7, 12649–12689, 2014

Calibration noise suppression for GLORIA

T. Guggenmoser et al.

Title Page

Abstract

Introduction

Conclusions

References

Tables

Figures



Back

Close

Full Screen / Esc

Printer-friendly Version

Interactive Discussion



Calibration noise suppression for GLORIA

T. Guggenmoser et al.

Title Page

Abstract

Introduction

Conclusions

References

Tables

Figures



Back

Close

Full Screen / Esc

Printer-friendly Version

Interactive Discussion



- Ridolfi, M., Stiller, G., and Zander, R.: MIPAS: an instrument for atmospheric and climate research, *Atmos. Chem. Phys.*, 8, 2151–2188, doi:10.5194/acp-8-2151-2008, 2008. 12651
- Friedl-Vallon, F., Maucher, G., Seefeldner, M., Trieschmann, O., Kleinert, A., Lengel, A., Keim, C., Oelhaf, H., and Fischer, H.: Design and characterization of the balloon-borne Michelson Interferometer for Passive Atmospheric Sounding (MIPAS-B2), *Appl. Optics*, 43, 3335–3355, 2004. 12651
- Friedl-Vallon, F., Gulde, T., Hase, F., Kleinert, A., Kulesa, T., Maucher, G., Neubert, T., Olschewski, F., Piesch, C., Preusse, P., Rongen, H., Sartorius, C., Schneider, H., Schönfeld, A., Tan, V., Bayer, N., Blank, J., Dapp, R., Ebersoldt, A., Fischer, H., Graf, F., Guggenmoser, T., Höpfner, M., Kaufmann, M., Kretschmer, E., Latzko, T., Nordmeyer, H., Oelhaf, H., Orphal, J., Riese, M., Schardt, G., Schillings, J., Sha, M. K., Suminska-Ebersoldt, O., and Ungermann, J.: Instrument concept of the imaging Fourier transform spectrometer GLORIA, *Atmos. Meas. Tech.*, 7, 3565–3577, doi:10.5194/amt-7-3565-2014, 2014. 12651, 12653
- Frigo, M. and Johnson, S. G.: FFTW: an adaptive software architecture for the FFT, in: *Proceedings of the 1998 IEEE International Conference on Acoustics, Speech and Signal Processing*, vol. 3, 1381–1384, IEEE, 1998. 12657
- Gettelman, A., Hoor, P., Pan, L., Randel, W., Hegglin, M., and Birner, T.: The extratropical upper troposphere and lower stratosphere, *Rev. Geophys.*, 49, RG3003, doi:10.1029/2011RG000355, 2011. 12650
- Grossmann, K. U., Offermann, D., Gusev, O., Oberheide, J., Riese, M., and Spang, R.: The CRISTA-2 mission, *J. Geophys. Res.*, 107, CRI 1–1–CRI 1–12, doi:10.1029/2001JD000667, 2002. 12651
- Guggenmoser, T.: *Data Processing and Trace Gas Retrievals for the GLORIA Limb Sounder*, vol. 230 of *Schriften des Forschungszentrums Jülich, Reihe Energie und Umwelt*, Forschungszentrum Jülich GmbH, Jülich, 2014. 12656
- Hoffmann, L., Kaufmann, M., Spang, R., Müller, R., Remedios, J. J., Moore, D. P., Volk, C. M., von Clarmann, T., and Riese, M.: Envisat MIPAS measurements of CFC-11: retrieval, validation, and climatology, *Atmos. Chem. Phys.*, 8, 3671–3688, doi:10.5194/acp-8-3671-2008, 2008. 12652
- Höpfner, M., Stiller, G. P., Kuntz, M., von Clarmann, T., Echle, G., Funke, B., Glatthor, N., Hase, F., Kemnitzer, H., and Zorn, S.: The Karlsruhe optimized and precise radiative transfer algorithm. Part II: Interface to retrieval applications, in: *Optical Remote Sensing of the At-*

Calibration noise suppression for GLORIA

T. Guggenmoser et al.

Title Page

Abstract

Introduction

Conclusions

References

Tables

Figures



Back

Close

Full Screen / Esc

Printer-friendly Version

Interactive Discussion



- Offermann, D., Grossmann, K.-U., Barthol, P., Knieling, P., Riese, M., and Trant, R.: Cryogenic Infrared Spectrometers and Telescopes for the Atmosphere (CRISTA) experiment and middle atmosphere variability, *J. Geophys. Res.*, 104, 16311–16325, 1999. 12651
- 5 Olschewski, F., Ebersoldt, A., Friedl-Vallon, F., Gutschwager, B., Hollandt, J., Kleinert, A., Monte, C., Piesch, C., Preusse, P., Rolf, C., Steffens, P., and Koppmann, R.: The in-flight blackbody calibration system for the GLORIA interferometer on board an airborne research platform, *Atmos. Meas. Tech.*, 6, 3067–3082, doi:10.5194/amt-6-3067-2013, 2013. 12654, 12659
- 10 Piesch, C., Gulde, T., Sartorius, C., Friedl-Vallon, F., Seefeldner, M., Wölfel, M., Blom, C., and Fischer, H.: Design of a MIPAS instrument for high-altitude aircraft, in: Presented at the Second International Airborne Remote Sensing Conference and Exhibition, vol. 24, p. 27, 1996. 12651
- Pyatykh, S., Hesser, J., and Zheng, L.: Image noise level estimation by principal component analysis, *IEEE T. Image Process.*, 22, 687–699, doi:10.1109/TIP.2012.2221728, 2013. 12660
- 15 Revercomb, H. E., Buijs, H., Howell, H. B., LaPorte, D. D., Smith, W. L., and Sromovsky, L.: Radiometric calibration of IR Fourier transform spectrometers: solution to a problem with the High-Resolution Interferometer Sounder, *Appl. Optics*, 27, 3210–3218, 1988. 12654
- 20 Riese, M., Preusse, P., Spang, R., Ern, M., Jarisch, M., Grossmann, U., and Offermann, D.: Measurements of trace gases by the Cryogenic Infrared Spectrometers and Telescopes for the Atmosphere (CRISTA) experiment, *Adv. Space Res.*, 19, 563–566, doi:10.1016/S0273-1177(97)00172-5, 1997. 12651
- Riese, M., Manney, G. L., Oberheide, J., Tie, X., Spang, R., and Küll, V.: Stratospheric transport by planetary wave mixing as observed during CRISTA-2, *J. Geophys. Res.*, 107, 8179, doi:10.1029/2001JD000629, 2002. 12651
- 25 Riese, M., Oelhaf, H., Preusse, P., Blank, J., Ern, M., Friedl-Vallon, F., Fischer, H., Guggenmoser, T., Höpfner, M., Hoor, P., Kaufmann, M., Orphal, J., Plöger, F., Spang, R., Suminska-Ebersoldt, O., Ungermann, J., Vogel, B., and Woiwode, W.: Gimballed Limb Observer for Radiance Imaging of the Atmosphere (GLORIA) scientific objectives, *Atmos. Meas. Tech.*, 7, 1915–1928, doi:10.5194/amt-7-1915-2014, 2014. 12650, 12651
- 30 Solomon, S., Rosenlof, K. H., Portmann, R. W., Daniel, J. S., Davis, S. M., Sanford, T. J., and Plattner, G.-K.: Contributions of stratospheric water vapor to decadal changes in the rate of global warming, *Science*, 327, 1219–1223, doi:10.1126/science.1182488, 2010. 12650

**Calibration noise
suppression for
GLORIA**

T. Guggenmoser et al.

Title Page

Abstract

Introduction

Conclusions

References

Tables

Figures



Back

Close

Full Screen / Esc

Printer-friendly Version

Interactive Discussion



Stiller, G. P. (Ed.): The Karlsruhe Optimized and Precise Radiative Transfer Algorithm (KOPRA), vol. 6487 of Wissenschaftliche Berichte des Forschungszentrums Karlsruhe, Forschungszentrum Karlsruhe, Karlsruhe, 2000. 12652

Ungermann, J., Kaufmann, M., Hoffmann, L., Preusse, P., Oelhaf, H., Friedl-Vallon, F., and Riese, M.: Towards a 3-D tomographic retrieval for the air-borne limb-imager GLORIA, Atmos. Meas. Tech., 3, 1647–1665, doi:10.5194/amt-3-1647-2010, 2010. 12652

Ungermann, J., Blank, J., Lotz, J., Leppkes, K., Hoffmann, L., Guggenmoser, T., Kaufmann, M., Preusse, P., Naumann, U., and Riese, M.: A 3-D tomographic retrieval approach with advection compensation for the air-borne limb-imager GLORIA, Atmos. Meas. Tech., 4, 2509–2529, doi:10.5194/amt-4-2509-2011, 2011. 12652

Ungermann, J., Kalicinsky, C., Olschewski, F., Knieling, P., Hoffmann, L., Blank, J., Woiwode, W., Oelhaf, H., Hösen, E., Volk, C. M., Ulanovsky, A., Ravegnani, F., Weigel, K., Stroh, F., and Riese, M.: CRISTA-NF measurements with unprecedented vertical resolution during the RECONCILE aircraft campaign, Atmos. Meas. Tech., 5, 1173–1191, doi:10.5194/amt-5-1173-2012, 2012. 12651

Ungermann, J., Pan, L. L., Kalicinsky, C., Olschewski, F., Knieling, P., Blank, J., Weigel, K., Guggenmoser, T., Stroh, F., Hoffmann, L., and Riese, M.: Filamentary structure in chemical tracer distributions near the subtropical jet following a wave breaking event, Atmos. Chem. Phys., 13, 10517–10534, doi:10.5194/acp-13-10517-2013, 2013. 12651

Ungermann, J., Blank, J., Dick, M., Ebersoldt, A., Friedl-Vallon, F., Giez, A., Guggenmoser, T., Höpfner, M., Jurkat, T., Kaufmann, M., Kaufmann, S., Kleinert, A., Krämer, M., Latzko, T., Oelhaf, H., Olschewski, F., Preusse, P., Rolf, C., Schillings, J., Suminska-Ebersoldt, O., Tan, V., Thomas, N., Voigt, C., Zahn, A., Zöger, M., and Riese, M.: Level 2 processing for the imaging Fourier transform spectrometer GLORIA: derivation and validation of temperature and trace gas volume mixing ratios from calibrated dynamics mode spectra, Atmos. Meas. Tech. Discuss., 7, 12037–12080, doi:10.5194/amtd-7-12037-2014, 2014. 12652

Weigel, K., Hoffmann, L., Günther, G., Khosrawi, F., Olschewski, F., Preusse, P., Spang, R., Stroh, F., and Riese, M.: A stratospheric intrusion at the subtropical jet over the Mediterranean Sea: air-borne remote sensing observations and model results, Atmos. Chem. Phys., 12, 8423–8438, doi:10.5194/acp-12-8423-2012, 2012. 12651

Woiwode, W., Oelhaf, H., Gulde, T., Piesch, C., Maucher, G., Ebersoldt, A., Keim, C., Höpfner, M., Khaykin, S., Ravegnani, F., Ulanovsky, A. E., Volk, C. M., Hösen, E., Dörnbrack, A., Ungermann, J., Kalicinsky, C., and Orphal, J.: MIPAS-STR measurements in the

AMTD

7, 12649–12689, 2014

Calibration noise suppression for GLORIA

T. Guggenmoser et al.

Title Page

Abstract

Introduction

Conclusions

References

Tables

Figures



Back

Close

Full Screen / Esc

Printer-friendly Version

Interactive Discussion



**Calibration noise
suppression for
GLORIA**

T. Guggenmoser et al.

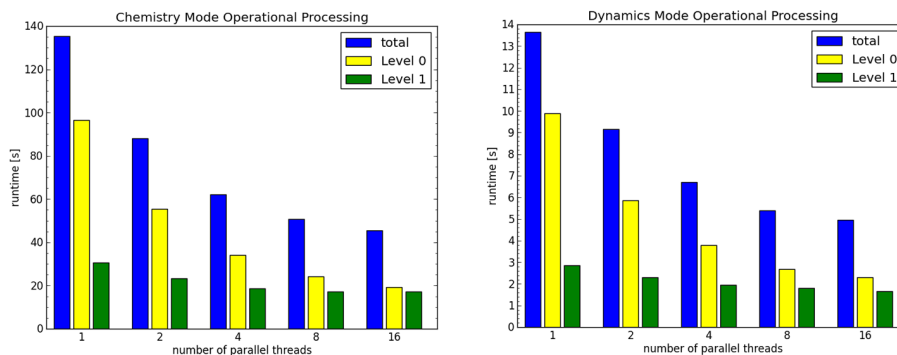


Figure 1. Runtime for the automated L0/L1 processor for different levels of parallelisation. In order to eliminate the influence of file input/output, the raw data were read from and the calibrated spectra written to a memory-based file system. Note that the L0 runtime as shown here encompasses the entire L0 processing stage, including the interferogram alignment correction. Earlier analyses of the operational L0 processor (Kleinert et al., 2014) showed the runtime for single execution.

[Title Page](#)[Abstract](#)[Introduction](#)[Conclusions](#)[References](#)[Tables](#)[Figures](#)[Back](#)[Close](#)[Full Screen / Esc](#)[Printer-friendly Version](#)[Interactive Discussion](#)

Calibration noise suppression for GLORIA

T. Guggenmoser et al.

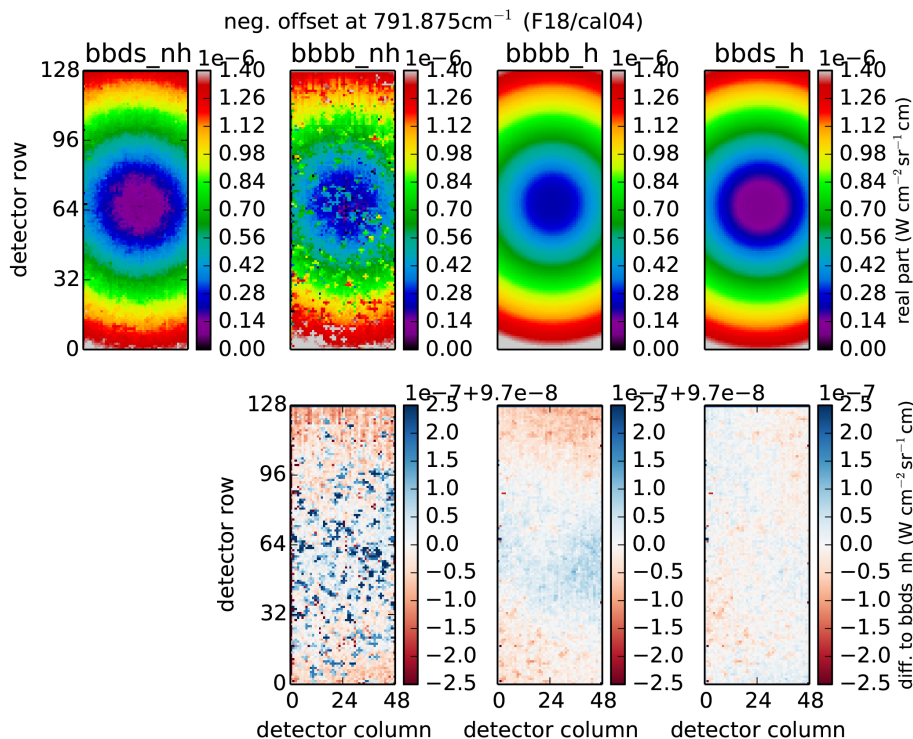


Figure 2. Real part of the NCO for different calibration methods at 791.875cm^{-1} . The leftmost image shows the BB-DS reference without pseudo-hyperbola fit. The following two are the values for the original BB-BB calibration and the corresponding pseudo-hyperbola, and the last panel shows an application of the pseudo-hyperbola to the BB-DS calibration. The images in the second row show the difference between the NCO values and those for the BB-DS reference.

Calibration noise suppression for GLORIA

T. Guggenmoser et al.

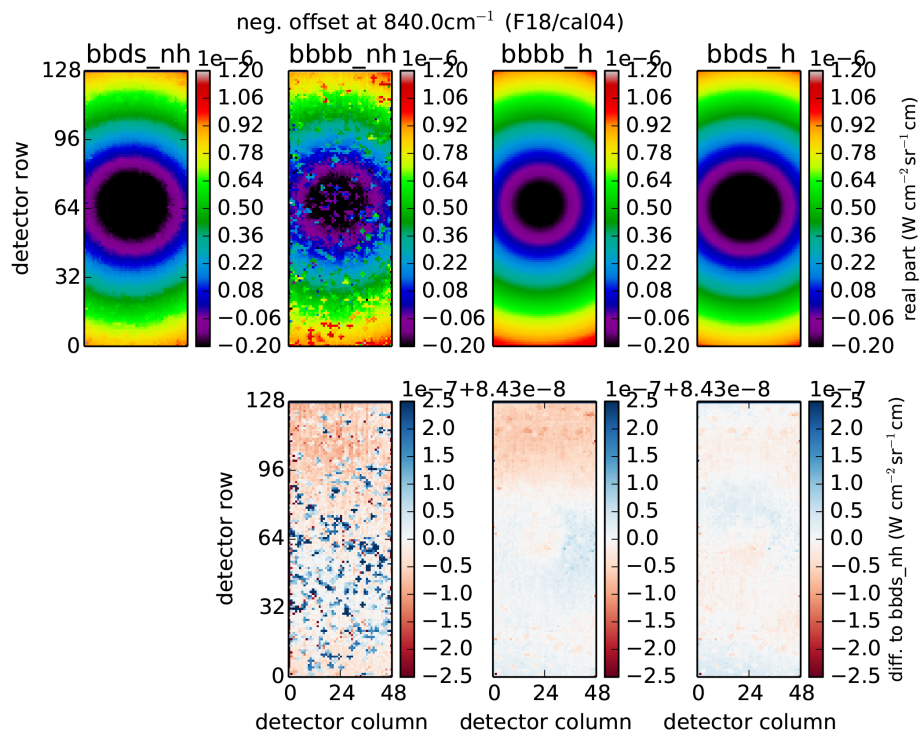


Figure 4. Real part of the NCO at 840.00 cm⁻¹, shown for the same calibration methods as in Fig. 2. Compared with the values at 791.875 cm⁻¹, this spectral sample cannot be as accurately reproduced using the pseudo-hyperbola fit.

Title Page

Abstract Introduction

Conclusions References

Tables Figures

◀ ▶

◀ ▶

Back Close

Full Screen / Esc

Printer-friendly Version

Interactive Discussion



Calibration noise suppression for GLORIA

T. Guggenmoser et al.

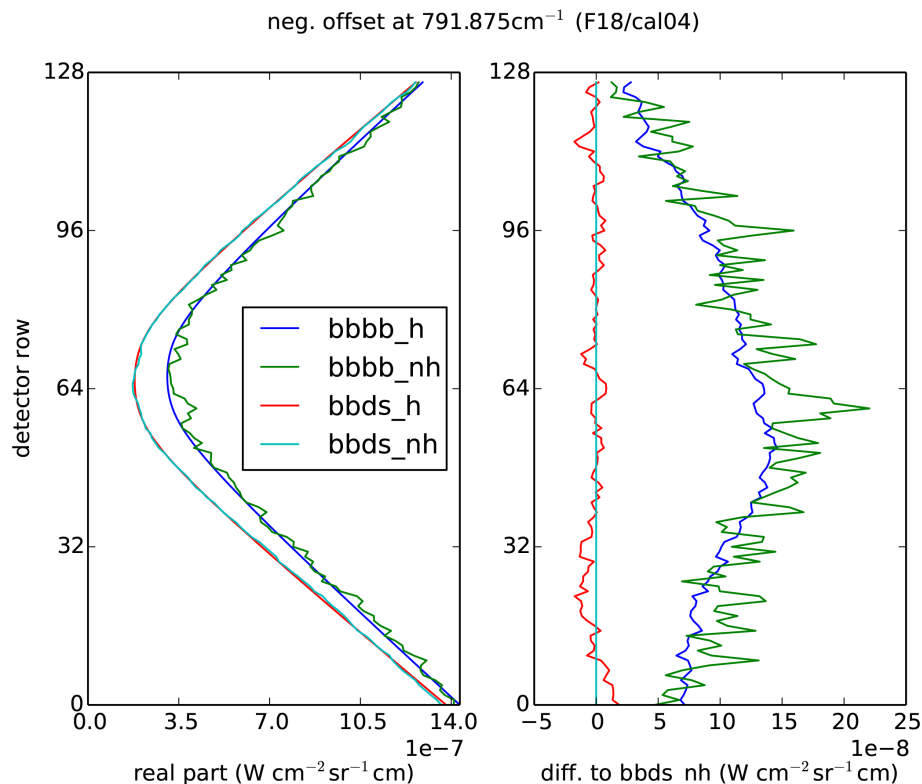


Figure 5. Averaged real part of the NCO over the detector rows for the different calibration methods. Both the unmodified data (suffix nh) and the pseudo-hyperbolas (suffix h) are shown. A discrepancy remains between the BB-DS and the BB-BB methods which has to be compensated for in the trace gas retrievals.

Title Page

Abstract

Introduction

Conclusions

References

Tables

Figures

◀

▶

◀

▶

Back

Close

Full Screen / Esc

Printer-friendly Version

Interactive Discussion



Calibration noise suppression for GLORIA

T. Guggenmoser et al.

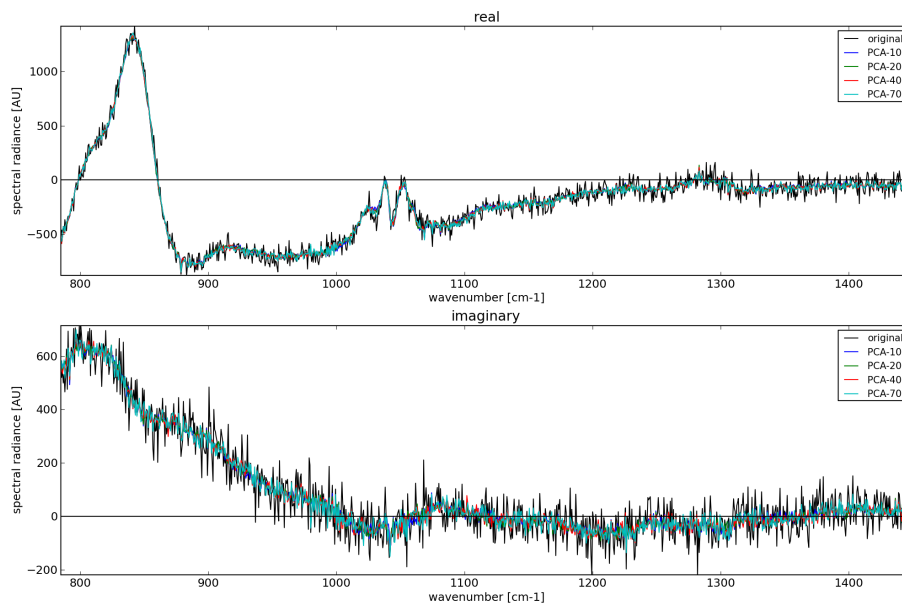


Figure 6. Reconstruction of a DS spectrum (centre pixel) from 10, 20, 40, and 70 principal components.

[Title Page](#)[Abstract](#)[Introduction](#)[Conclusions](#)[References](#)[Tables](#)[Figures](#)[◀](#)[▶](#)[◀](#)[▶](#)[Back](#)[Close](#)[Full Screen / Esc](#)[Printer-friendly Version](#)[Interactive Discussion](#)

Calibration noise suppression for GLORIA

T. Guggenmoser et al.

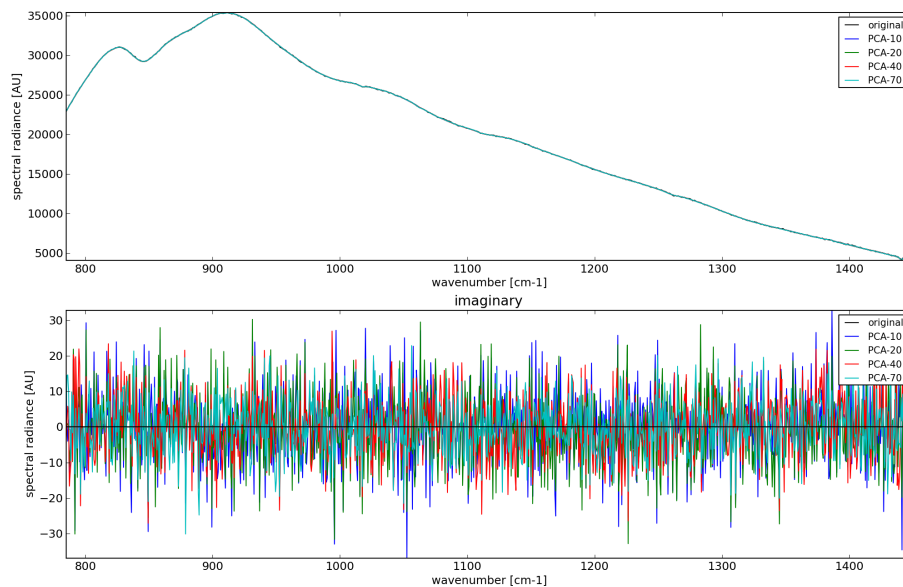


Figure 7. Reconstruction of a BB spectrum (centre pixel) from 10, 20, 40, and 70 principal components.

[Title Page](#)[Abstract](#)[Introduction](#)[Conclusions](#)[References](#)[Tables](#)[Figures](#)[◀](#)[▶](#)[◀](#)[▶](#)[Back](#)[Close](#)[Full Screen / Esc](#)[Printer-friendly Version](#)[Interactive Discussion](#)

Calibration noise suppression for GLORIA

T. Guggenmoser et al.

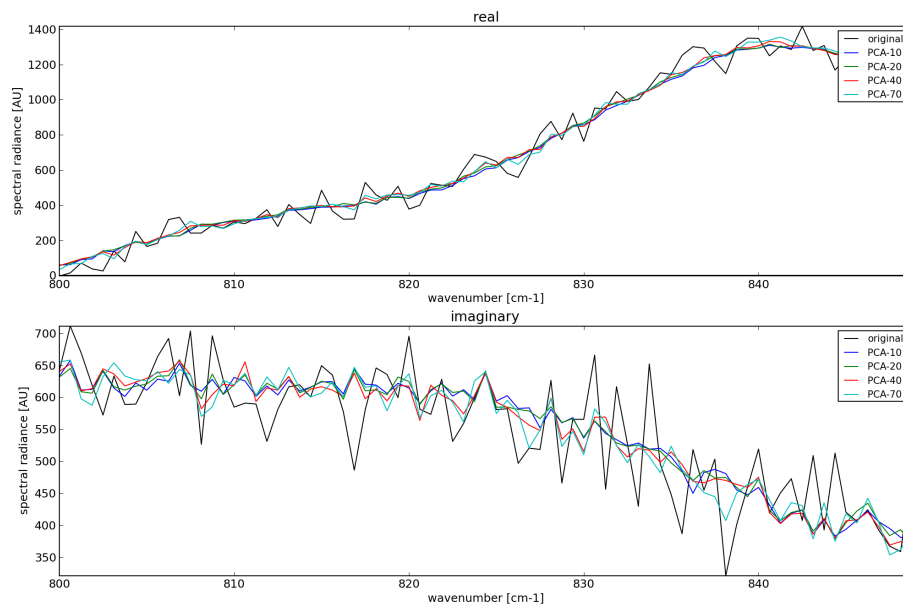


Figure 8. The same reconstructions as in Fig. 6, but in a limited spectral range between 800 and 850 cm^{-1} .

[Title Page](#)[Abstract](#)[Introduction](#)[Conclusions](#)[References](#)[Tables](#)[Figures](#)[◀](#)[▶](#)[◀](#)[▶](#)[Back](#)[Close](#)[Full Screen / Esc](#)[Printer-friendly Version](#)[Interactive Discussion](#)

Calibration noise suppression for GLORIA

T. Guggenmoser et al.

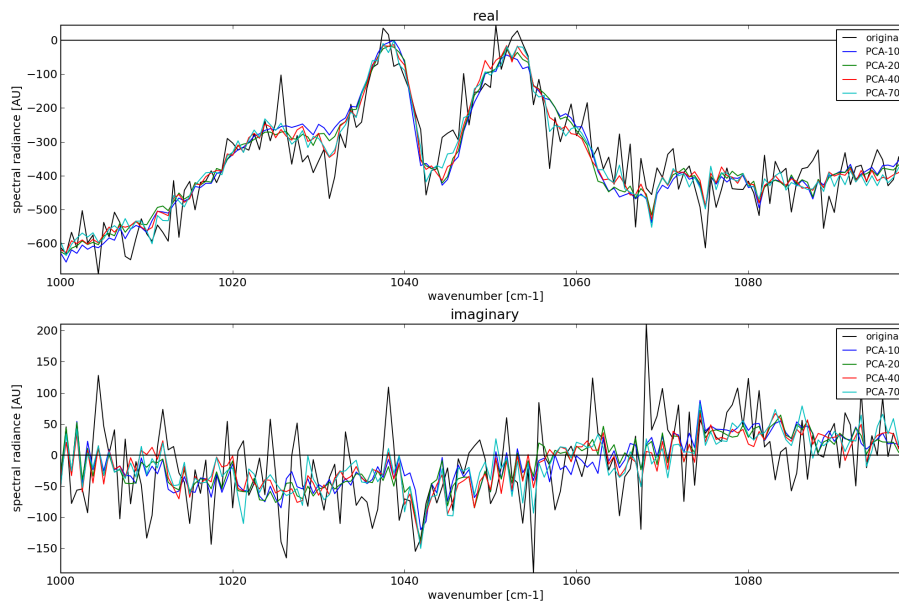


Figure 9. Reconstructions of the same DS spectrum as in Figs. 6 and 8, in the spectral range between 1000 and 1100 cm^{-1} . The obvious discrepancies between the reconstructions and the original spectrum are due to residual emissions from stratospheric trace gases.

[Title Page](#)[Abstract](#)[Introduction](#)[Conclusions](#)[References](#)[Tables](#)[Figures](#)[◀](#)[▶](#)[◀](#)[▶](#)[Back](#)[Close](#)[Full Screen / Esc](#)[Printer-friendly Version](#)[Interactive Discussion](#)

**Calibration noise
suppression for
GLORIA**

T. Guggenmoser et al.

Title Page

Abstract

Introduction

Conclusions

References

Tables

Figures



Back

Close

Full Screen / Esc

Printer-friendly Version

Interactive Discussion

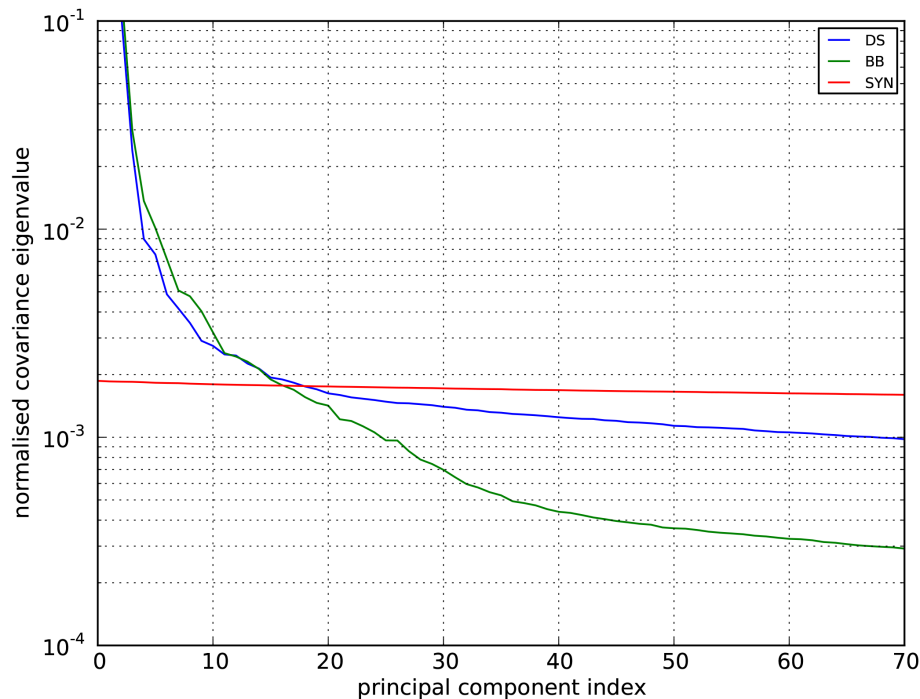


Figure 10. Normalised covariance eigenvalues of a DS, BB, and synthetic white noise data set. The eigenvalues indicate the rate at which each successive principal component adds to the total variance.

**Calibration noise
suppression for
GLORIA**

T. Guggenmoser et al.

Title Page

Abstract

Introduction

Conclusions

References

Tables

Figures

◀

▶

◀

▶

Back

Close

Full Screen / Esc

Printer-friendly Version

Interactive Discussion

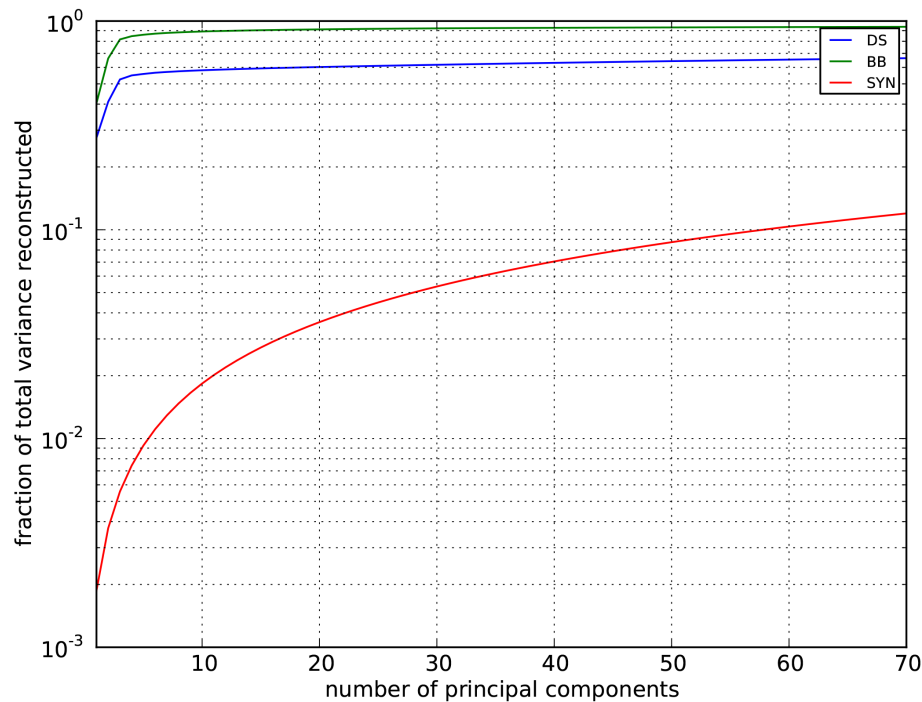
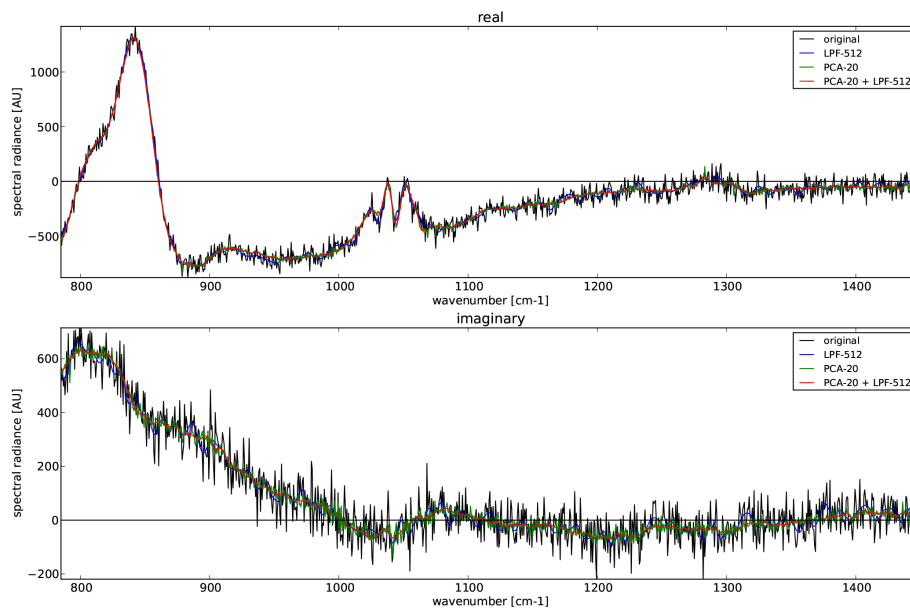


Figure 11. Cumulative normalised covariance eigenvalues, i.e. the cumulative sum of the values shown in Fig. 10. These indicate the relative variance restored after reconstructing the image from a given number of principal components.

**Calibration noise
suppression for
GLORIA**

T. Guggenmoser et al.

**Figure 12.** Comparison between the PCA, low-pass and combined noise suppression methods.[Title Page](#)[Abstract](#)[Introduction](#)[Conclusions](#)[References](#)[Tables](#)[Figures](#)[◀](#)[▶](#)[◀](#)[▶](#)[Back](#)[Close](#)[Full Screen / Esc](#)[Printer-friendly Version](#)[Interactive Discussion](#)

Calibration noise suppression for GLORIA

T. Guggenmoser et al.

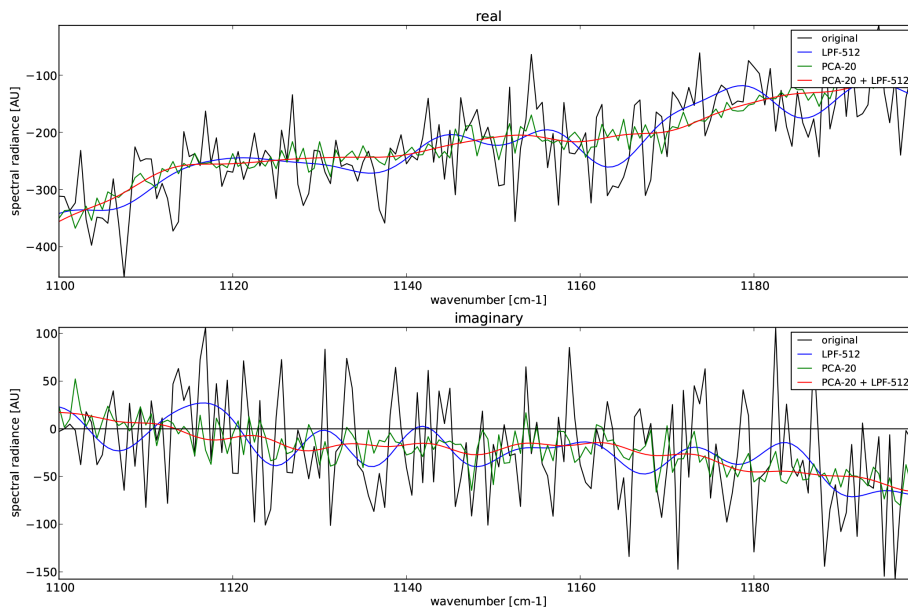


Figure 13. Comparison between the PCA, low-pass and combined noise suppression methods in the spectral range between 1100 and 1200 cm^{-1} . The pure low-pass method retains higher amounts of low-frequency noise, which manifest as slow oscillations in the spectrum. The PCA method subtracts noise variance irrespective of frequency (see also Fig. 15).

[Title Page](#)[Abstract](#)[Introduction](#)[Conclusions](#)[References](#)[Tables](#)[Figures](#)[◀](#)[▶](#)[◀](#)[▶](#)[Back](#)[Close](#)[Full Screen / Esc](#)[Printer-friendly Version](#)[Interactive Discussion](#)

**Calibration noise
suppression for
GLORIA**

T. Guggenmoser et al.

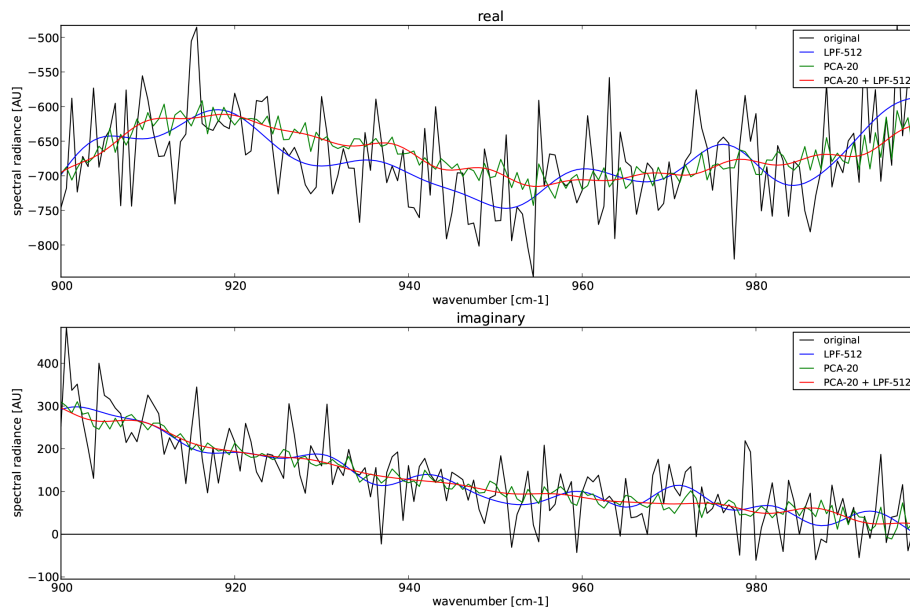


Figure 14. Comparison between the PCA, low-pass and combined noise suppression methods in a limited spectral range. Between 920 and 960 cm^{-1} , a small bias appears between the PCA methods and the pure LPF method. This bias is still within the original spectrum's noise range.

Title Page

Abstract

Introduction

Conclusions

References

Tables

Figures

◀

▶

◀

▶

Back

Close

Full Screen / Esc

Printer-friendly Version

Interactive Discussion



**Calibration noise
suppression for
GLORIA**

T. Guggenmoser et al.

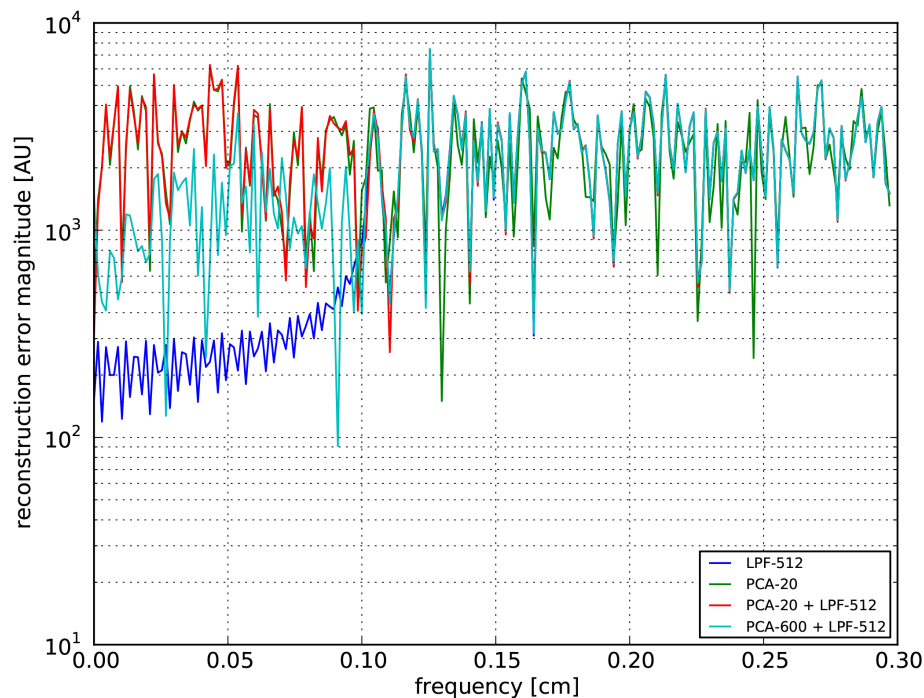


Figure 15. Spectrum of the reconstruction error, i.e. the difference between the processed and the original spectrum, for different noise suppression methods. Shown are only the low frequencies. The LPF subtracts high frequency noise from the spectrum, which means that low-frequency noise modes are retained. The PCA method introduces no such bias. The combined PCA + LPF method introduces no noticeable bias as long as the number of principal components is kept small. Note that the abscissa is in spatial units; this is because it is the Fourier space associated with the wavenumber space.

[Title Page](#)[Abstract](#)[Introduction](#)[Conclusions](#)[References](#)[Tables](#)[Figures](#)[Back](#)[Close](#)[Full Screen / Esc](#)[Printer-friendly Version](#)[Interactive Discussion](#)